Simple low-power demodulator for the measurement of basal and physiological changes of electrical bioimpedance

Ernesto Serrano-Finetti
Instrumentation, Sensors and Interfaces Group, Dept. of Electronic Engineering
Universitat Politècnica de Catalunya
Castelldefels, Spain
ernesto.serrano@upc.edu

Gemma Hornero
Instrumentation, Sensors and Interfaces Group, Dept. of Electronic Engineering
Universitat Politècnica de Catalunya
Castelldefels, Spain
gemma.hornero@upc.edu

Oscar Casas
Instrumentation, Sensors and Interfaces Group, Dept. of Electronic Engineering
Universitat Politècnica de Catalunya
Castelldefels, Spain
jaime.oscar.casas@upc.edu

Abstract—**Wearable sensors constitute a growing trend both as a research tool as well as an end-consumer products. In the physiological signal monitoring fields, the changing signals have a low bandwidth hence most sensing techniques are not power-hungry. Electrical bioimpedance is a non-obtrusive sensing technique and is an interesting choice as it can recover both breathing and pulse rate signals. However, it works at comparatively higher frequencies and usually need demodulation circuitry, meaning higher power consumption. In this work, we show an alternative technique to demodulate the impedance response that need very few components and whose power consumption can be tailored as needed. We show that, by using a 24-bit ADC, the respiration and pulse rate signals as well as the basal impedance are recovered from the demodulated signal and further digital band-pass filters that are easily implemented with currently available low-power microcontroller technology. Further, it constitutes a compact solution, as the sensor needs not to change location to measure these signals.**

Keywords—wearable sensors, low-power, amplitude demodulation, impedance sensor, pulse rate, respiratory rate.

I. INTRODUCTION

Wearable sensors constitute an interesting choice in physiological signal monitoring applications either as research tools or as end-consumer products. Most signals of interest occupy a relatively small signal bandwidth like temperature, ECG and activity; hence, the corresponding analog processing circuits (amplifiers, filters, etc.) are usually not power-hungry. In non-clinical applications like patient monitoring at home, heart/pulse rate (HR) and respiration rate (ResR) are two signals of interest that are usually acquired with different devices or sensors [1]. Most long-term HR monitoring solutions are based on photoplethysmography (PPG) because it integrates easily into wearable devices like smartphones. However, PPG sensors need a light source –an LED– hence its power consumption is not as low as desirable. One way to reduce its power consumption is to decrease its duty cycle, and even adapt it to skip some heartbeats whenever the HR is stable and low, increasing it only when the detected HR increases [2]. Nonetheless, PPG provides only HR and sometimes ResR with the appropriate signal processing. Proposals of wearable sensors to acquires RespR signals include strain sensors [3], temperature sensors [4] and accelerometers [5], to name some. Their power budgets are tailored to be as low as desired but, again, they are only able to deliver a respiratory signal.

Electrical bioimpedance (EBI) is a non-obtrusive technique able to provide information on the electrical properties of tissues. The same sensors are able to provide information about the basal impedance of a body segment or body location (i.e. skin hydration) as well as its changes over time. Specifically, any physiological change like cardiac or respiratory activity can also be tracked with this technique. This technique is gaining attraction not only for benchtop applications but also for wearable devices [6]. Power consumption minimization is a requirement in a wearable sensor scenario. There are already low-power EBI measurement systems in the relevant literature but they usually rely on some type of synchronous rectifier demodulator ([7], [8]) or even in digital demodulation [9].

Switching the power supply of a signal amplifier has been used in [10] as a modulation technique to reduce both power consumption and low-frequency noise. Our approach is similar, but now applied to the demodulator stage. In this work, we propose the use of a demodulator consisting of a fully-differential amplifier (FDA) turned on and off synchronously with the excitation carrier. This makes the FDA perform as a mixer, multiplying the input with a 0 to G square-wave gain that serves as the reference "signal". The recovered impedance response is usually very small and requires either amplification or a high resolution digitizer. The latter is used in this work to show the feasibility of the proposed demodulated technique to measure the tiny impedance changes produced by respiration and cardiac activity, which enables HR and RespR monitoring.

II. MATERIALS AND METHODS

A. Demodulation technique

Fig. 1 shows the proposed analog front-end (AFE) demodulator for bioimpedance measurements. OA1 and OA2 are two op amps configured as a FDA with gain

$$G_{\mathrm{d}} = 1 + 2R_f/R_g , \qquad (1)$$

and that have shutdown capability. $v_{\mathrm{pd}}(t)$ is a square wave signal synchronized to the sinusoidal excitation carrier, $v_{\mathrm{c}}(t)$, with frequency $f_{\mathrm{c}} = 1/T_{\mathrm{c}}$. The op amps are enabled when $v_{\mathrm{c}}(t) > 0$ and are disabled otherwise. Therefore, this circuit mixes $v_{\mathrm{z}}(t)$ –the impedance response– and the time-dependent gain, $G(t)$

$$G(t) = \begin{cases} G_{\mathrm{d}}, & 0 \le t < T_{\mathrm{c}}/2 \\ 0, & T_{\mathrm{c}}/2 < t \le T_{\mathrm{c}} \end{cases} . \qquad (2)$$
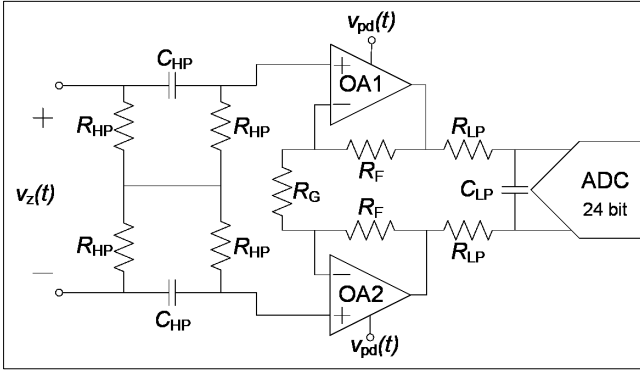
272

Figure 1. Analog front-end for the bioimpedance signal ($v_z(t)$) demodulation, where the gain is controlled by $v_{pd}(t)$ synchronously to the carrier signal, $v_c(t)$.

This technique is analogous to using a synchronous rectifier using a square wave gain of ±1, changing synchronously to $v_c(t)$. However, here $G(t)$ –the reference signal- produces a half-wave rectified signal hence it loses half of the signal power as compared to the ±1 gain but also reduces the demodulator power consumption to the half. On the other hand, $G(t)$ has an offset and, when making measurements on an individual, any biopotential signal (like the ECG) is amplified and will be superposed to the demodulated output. To avoid this, a differential high-pass filter (1st order) is included at the input with cutoff frequency f_L,

$$f_L = 1/(2\pi R_{HP} C_{HP}),\qquad(3)$$

and is chosen to be a decade lower than f_c. For example, if $f_c = 10$ kHz then $f_L = 1$ kHz, which offers attenuation better than 20 dB at the QRS ECG complex (between 20 Hz and 50 Hz). The half-wave rectified signal is then passed to a differential 1st order low-pass filter with cutoff frequency f_H,

$$f_H = 1/(4\pi R_{LP} C_{LP}).\qquad(4)$$

B. Four-electrode measurements with a voltage divider

Instead of using a current source to drive the excitation, we applied $v_c(t)$ to a voltage divider constituted by the measured body segment $Z_b(t)$, a reference resistor R_o and the injection electrodes with impedances Z_{e1} and Z_{e2}. Two other electrodes (Z_{e3} and Z_{e4}) picked up the body impedance response, $v_z(t)$, as shown in fig. 2. With this approach, less active components are used hence the expenses of cost power consumption and space are reduced. Conventional ECG clamp electrodes were used, and ECG gel was applied to reduce contact impedance.
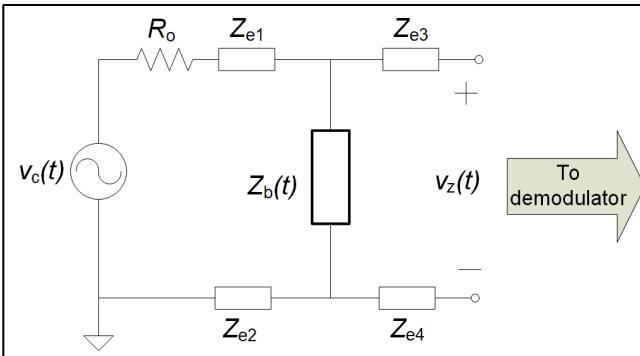

Figure 2. Voltage divider technique applied to bioimpedance measurements with four electrodes. R_o is a current limiting resistor, and $v_z(t)$ is the bioimpedance response signal.

C. Circuit implementation and performance test

OA1 and OA2 in Fig. 1 were the OPA363 op amp (Texas Instruments, Inc.), whose main characteristics are a 7 MHz gain-bandwidth product, a slew rate of 5 V/μs and a voltage noise density of 17 nV/√Hz at 10 kHz. The FDA gain was $G_d = 25$ ($R_f = 180$ kΩ, $R_g = 15$ kΩ) and it was supplied from a 5 V single power supply. A virtual ground circuit was set at half the power supply by means of a voltage divider and a buffer based on the LMV118 op amp (Texas Instruments, Inc.) The carrier frequency was set at 10 kHz hence $f_L = 1$ kHz, and to recover the cardiac impedance signal we set $f_H = 20$ Hz.

$v_c(t)$ and $v_{pd}(t)$ were generated with the Keysight 33212A function generator (Keysight Technologies). The excitation signal was a 10 kHz sine wave with an amplitude of 2 V, and the power-down signal changed synchronously to the carrier frequency between 0 V and 5 V to disable and enable OA1 and OA2, respectively. R_o was set at 2 kΩ hence the maximum current cannot surpass an amplitude of 1 mA in any case. The AFE output was digitized with an ADS1299 (Texas Instruments, Inc.) This circuit is a low-power, low noise 24-bit, simultaneously sampling, eight-channel front-end for the acquisition of biosignals. For this work, it has been programmed with a sampling frequency of 250 Hz and internal gain $G_{ADC} = 1$. The data output is communicated via SPI to an STM32L4R5 microcontroller (ST Microelectronics). Fig. 3 shows both the ADS1299 and the STM32L4R5 used. The latter is in charge of controlling the data communication to a laptop (USB) and of setting the registers to optimize the data acquisition performed with a custom-made LabVIEW application (National Instruments Corp.) Fig. 4 shows the block diagram of this data acquisition system. All resistors used had 1% tolerance, and the capacitors had a 5% tolerance.
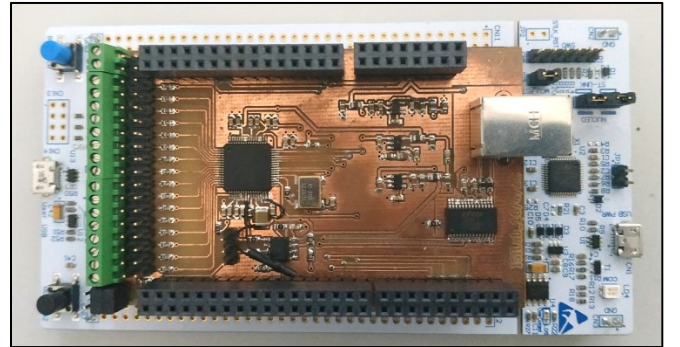

Figure 3. Printed circuit boards for the ADS1299 and the STM32L4R5 used for data acquisition of the AFE output.
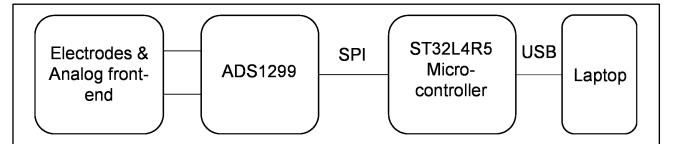

Figure 4. Block diagram of the data acquisition system used in this work.

Once implemented, the common-mode rejection ratio (CMRR) was measured. In applications like biopotentials or bioimpedance, where there is the need to use electrodes, the electrode-skin interface introduces a series contact impedance whose mismatch decreases the CMRR of the amplifier alone [11]. Therefore, an impedance of 100 kΩ∥10 nF was placed in series to one of the FDA inputs as shown in fig. 5 to simulate a worst-case scenario of electrode contact impedance

273

mismatch. The common mode signal $v_{CM}(t)$ was a 1 V, 10 kHz amplitude sinusoidal signal.
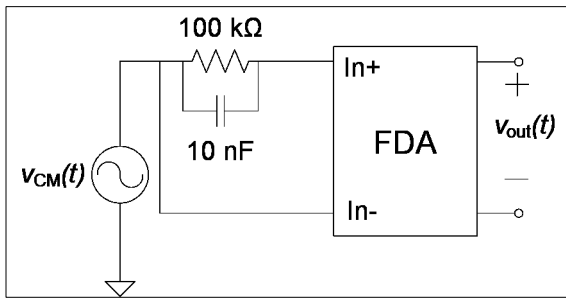

Figure 5. Experimental setup for the FDA's CMRR measurement.

The injected current was also tested by measuring the voltage drop in R_o and applying Ohm's law.

D. Signal processing

The high resolution of the ADC and the signal bandwidth from 0 to 20 Hz allow to recover both the respiratory and pulse rate signals by means of band-pass digital filtering in MatLab® (The Mathworks, Inc.). The characteristics of the filters are:

a) Respiration: A high-pass filter of order 2 and 0.1 Hz cutoff frequency, followed by a low-pass filter of 4th order and 1 Hz cutoff frequency.

b) Pulse rate: A high-pass filter of order 2 and 0.5 Hz cutoff frequency, followed by a low-pass filter of 4th order and 8 Hz cutoff frequency.

E. Measurement protocol

We asked 3 healthy volunteers to perform a deep and fast breathing pattern while wearing two conventional ECG clamp electrodes on each arm such that there was one injector electrode and one pickup electrode on each arm. After the measurements, we extracted the HR and RespR signals following the signal processing described in the previous subsection.

III. RESULTS AND DISCUSSION

A. Circuit performance

The measured CMRR was 67.2 dB, mainly due to the impedance introduced to simulate the impedance mismatch as occurs in a practical situation. It certainly is a worst-case scenario, which usually corresponds to situation found at the beginning of the measurements with dry electrodes. After electrode settling, this mismatch will tend to decrease. The FDA alone had a CMRR of 79.8 dB so the actual CMRR will lie between these two values. Additional information about the capability of this circuit to measure a static complex impedance is found in [12].

The voltage drop on R_o was 0.5 V rms hence the injected current was about 250 μA rms, well below the electrical security standards (IEC60601). This value relies heavily on the electrode-skin contact impedance but was deemed appropriate as it was not a device for medical use nor the volunteers had any medical condition that prevented the bioimpedance measurements.

B. Measurements on healthy volunteers

Fig. 6 shows the low-pass filtered signal containing the respiratory signal, in arbitrary units. The forced deep breathing pattern can be clearly observed. This signal constitutes about 10% of the basal impedance, and usually lower resolution ADCs are enough. However, the cardiac signal component is about 0.1 % of the basal impedance hence it needs further band-pass filtering, usually between 0.5 Hz and 5 Hz, and a large amplification prior to digitization. Another approach –followed in this work– is to use a higher resolution ADC (24 bits in our case). It not only avoids the use of more components but also saves acquisition time by avoiding the transients associated with low high-pass cutoff frequency. Therefore, the measurement system consumes less power.
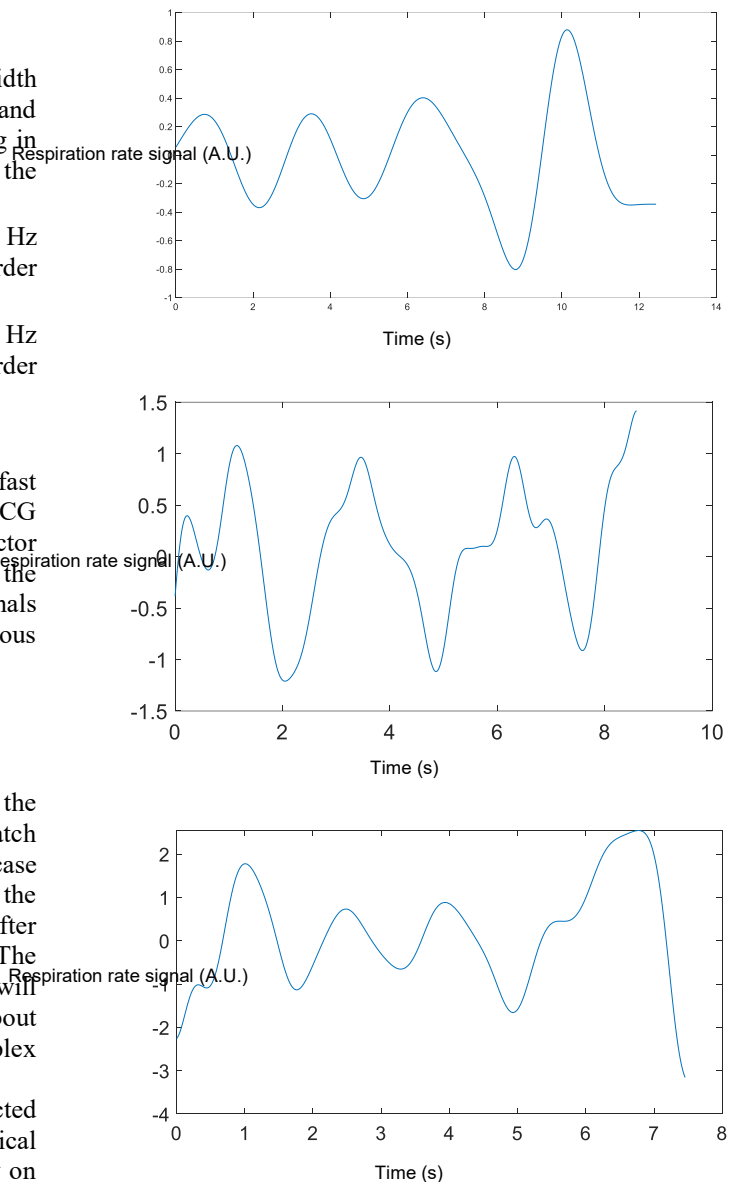

Figure 6. Respiration signal (in arbitrary units) from 3 healthy volunteers, recovered with a low-pass digital filter. The respiration pattern was forced.

Fig. 7 shows the recovered cardiac signal after band-pass filtering. This signal shows clearly defined peaks and is useful to calculate the pulse rate. It must be noted that the signals shown are not expressed in ohms, as the only interest of this work was to show the feasibility of this technique in

274

recovering the variations of impedance where the HR and RespR signals can be extracted. A proper calibration of the system was out of the scope of this work.

All of the respiratory signals had enough quality as to enable the measurement of respiratory rate. However, in one of the volunteers, the cardiac signal was irregular. The pressure wave is at the origin of the cardiac impedance signals hence it is expected that it exhibit the same features (for example, the dicrotic notch). On two of the volunteers these features were present, and all of them had clearly recognizable peaks thus HR can be obtained.

From the point of view of power consumption, our proposal saves 50 % of the power consumed by the conventional demodulators using square-waves as a reference signal as it is active only 50 % of the time. However, it even saves more power by avoiding the use of more active components usually found in similar demodulation circuitry.
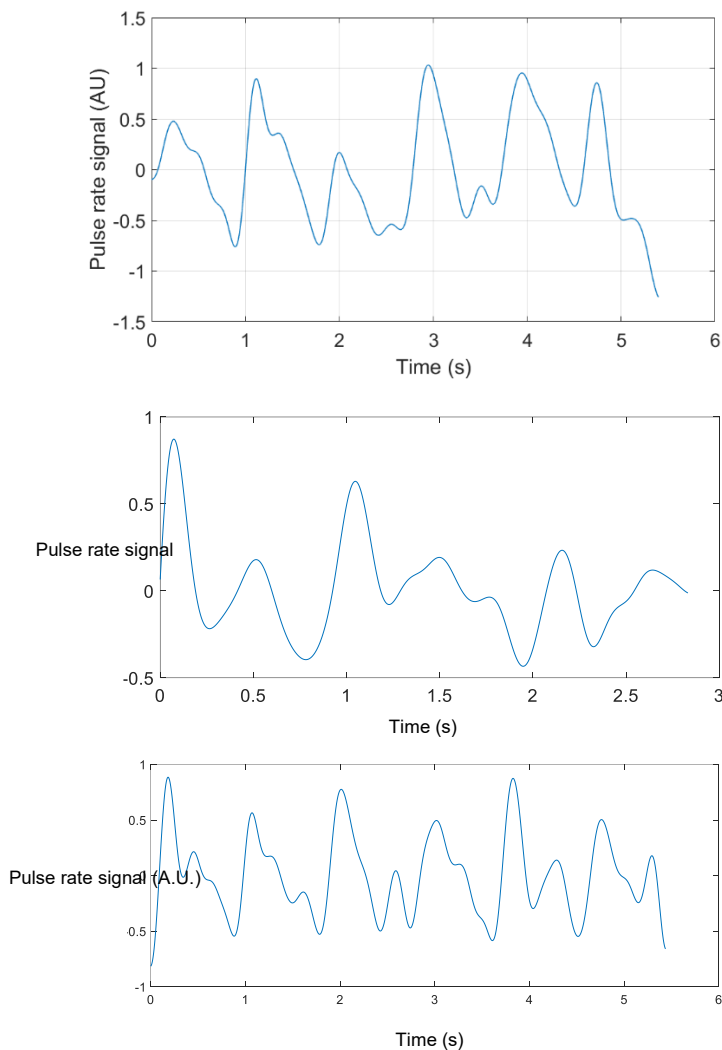

Figure 7. Pulse rate signal (in arbitrary units) recovered from 3 healthy volunteers with a digital band-pass filter.

Measuring bioimpedance with a voltage divider simplifies the design and avoids the use of more active components to implement a current injector. However, it also makes it more susceptible to baseline wandering due to the movement of the current injecting electrodes, making it necessary to apply digital filtering. In this way, the main features clearly arise in the filtered signals. Currently available microcontrollers can perform this processing at low power consumption.

This particular AFE implementation has a power consumption around 1.6 mA. OA1 and OA2 consume about 1 mA each but are active halt of the time, and the voltage splitter consumes about 0.6 mA. The effective current flowing through the body is less than 100 μA and is limited by the electrode impedance. At 5 V, its power consumption is in the order of 8 mW which can be reduced to less than 3 mW by using the minimum supply voltage of 1.8 V. Power consumption reduction mainly depends on the op amps, and there exist lower power alternatives that can fit lower power budgets. This will be done at the expense of a lower gain-bandwidth product that means a trade-off between the FDA gain and the carrier frequency.

The main advantage of this AFE is that it is able to give three different magnitudes –basal impedance, respiration changes and cardiac changes– without changing the sensor location. Basal impedance yields information about the health status of the tissues of a body segment, like in body composition studies. Moreover, the ability to follow cardiac and respiratory changes allows calculating the pulse rate and the respiratory rate with readily available algorithms, and enables the development of small sensors –like a patch– placed unobtrusively on the body, without disturbing the normal activities of a person.

IV. CONCLUSIONS

We have shown an alternative solution to conventional bioimpedance demodulators that allows saving power consumption, space and costs by using very few components. Thanks to the use of a 24-bit ADC, breath and pulse rate are recovered from the same demodulated signal. Moreover, the application of a voltage divider avoids the implementation of a current injector further reducing power consumption. At the same time, this injection strategy makes the system somewhat more susceptible to electrode movement. Straightforward digital filtering remediates these movement artifacts and allows the selection of the respiration and pulse rate signals.

This AFE solution enables the development of compact solutions for wearable sensors aimed at keeping track of the health status –pulse and respiratory rates–, and its power consumption can be tailored to a low-power source like a small battery.

REFERENCES

[1] L. Ke, L. Yang, F. Seoane, F. Abtahi, M. Forsman, and K. Lindecrantz, "Fusion of heart rate, respiration and motion measurements from a wearable sensor system to enhance energy expenditure estimation," *Sensors (Switzerland)*, vol. 18, no. 9, Sep. 2018, doi: 10.3390/s18093092.

[2] Z. Ma *et al.*, "A Low-Power Heart Rate Sensor with Adaptive Heartbeat Locked Loop," Apr. 2021, pp. 1–5. doi: 10.1109/iscas51556.2021.9401726.

[3] M. Chu *et al.*, "Respiration rate and volume measurements using wearable strain sensors," *npj Digital Medicine*, vol. 2, no. 1, Dec. 2019, doi: 10.1038/s41746-019-0083-3.

[4] Y. Xu, Q. Li, Z. Tang, J. Liu, and B. Xiang, "Towards accurate, cost-effective, ultra-low-power and non-invasive respiration monitoring: A

275

reusable wireless wearable sensor for an off-the-shelf KN95 mask," *Sensors*, vol. 21, no. 20, Oct. 2021, doi: 10.3390/s21206698.

[5]   I. Degtyarenko, K. Slyusarenko, A. Omelchenko, V. Riabov, and S. Chyzhyk, "LOW-POWER CONTINUOUS HEART AND RESPIRATION RATES MONITORING ON WEARABLE DEVICES," in *2018 IEEE International Conference on Acoustics, Speech and Signal Processing : proceedings*, 2018, pp. 1298–1302.

[6]   J. Xu and Z. Hong, "Low Power Bio-Impedance Sensor Interfaces: Review and Electronics Design Methodology," *IEEE Reviews in Biomedical Engineering*, vol. 15, pp. 23–35, 2022, doi: 10.1109/RBME.2020.3041053.

[7]   K. Kim, M. Kim, H. Cho, K. Lee, S. T. Ryu, and H. J. Yoo, "A 54-µW fast-settling arterial pulse wave sensor for wrist watch type system," in *Proceedings - IEEE International Symposium on Circuits and Systems*, Jul. 2016, vol. 2016-July, pp. 1082–1085. doi: 10.1109/ISCAS.2016.7527432.

[8]   S. Rodriguez, S. Ollmar, M. Waqar, and A. Rusu, "A Batteryless Sensor ASIC for Implantable Bio-Impedance Applications," *IEEE Transactions on Biomedical Circuits and Systems*, vol. 10, no. 3, pp. 533–544, Jun. 2016, doi: 10.1109/TBCAS.2015.2456242.

[9]   K. Sel, B. Ibrahim, and R. Jafari, "ImpediBands: Body Coupled Bio-Impedance Patches for Physiological Sensing Proof of Concept," *IEEE Transactions on Biomedical Circuits and Systems*, vol. 14, no. 4, pp. 757–774, Aug. 2020, doi: 10.1109/TBCAS.2020.2995810.

[10]   G. Hornero, O. Casas, and R. Pallàs-Areny, "Signal to noise ratio improvement by power supply voltage switching," in *16th IMEKO TC4 Symposium Exploring New Frontiers of Instrumentation and Methods for Electrical and Electronic Measurements*, 2008, pp. 1–6. Accessed: Jan. 12, 2022. [Online]. Available: https://www.imeko.org/publications/tc4-2008/IMEKO-TC4-2008-149.pdf

[11]   Ó. Casas and R. Pallás-Areny, "Basics of analog differential filters," *IEEE Transactions on Instrumentation and Measurement*, vol. 45, no. 1, pp. 275–279, 1996, doi: 10.1109/19.481347.

[12]   E. Serrano-Finetti, G. Hornero, and O. Casas, "Complex impedance measurement front-end based on an on/off lock-in amplifier," in *2022 IEEE International Workshop on Metrology for Industry 4.0 & IOT*, 2022, pp. 1–5. (Accepted)

276